Attosecond probing of photoionization dynamics from diatomic to many-atom molecules

Alexie Boyer, Saikat Nandi, Vincent Loriot

Attosecond probing of photoionization dynamics from diatomic to many-atom molecules

Alexie Boyer, Saikat Nandi and Vincent Loriot

University of Lyon, Université Claude Bernard Lyon 1, CNRS, Institut Lumière Matière, VILLEURBANNE, F-69622, France.

*Corresponding author(s). E-mail(s): vincent.loriot@univ-lyon1.fr;
Contributing authors: alexie.boyer@univ-lyon1.fr;
saikat.nandi@univ-lyon1.fr;

Abstract

The natural diversity of molecules in terms of geometries, chemical properties, work-functions, among others, offers an impressive laboratory for observing fundamental electron dynamics down to the attosecond timescale. Here, we use some recent angularly resolved Wigner time delay measurements performed in our attoscience laboratory in Lyon to illustrate the electron dynamics in molecules containing a few (N_2, C_2H_2, and C_2H_4) to many atoms ($C_{10}H_8$ and $C_{10}H_{16}$). In the few-atom case, the Wigner delay can be measured for a particular electronic state. This allows us to identify the underlying physical mechanisms governing photoionization processes, such as the well-known shape resonance in valence-ionized nitrogen molecule. Promising new experimental results using angle-resolved photoelectron spectroscopy on ethylene show a tendency in the ionization time delay between the $\boldsymbol{X}$ and $\boldsymbol{A}$ states. As a perspective, we show that for many-atom molecules (C_{60} and $C_{10}H_{\boldsymbol{x}}$, with $\boldsymbol{x} = \mathbf{8}$ or $\mathbf{16}$), the photoionization metrology can address different kinds of electron dynamics with a collective behavior.

Keywords: Attoscience, RABBIT measurements, Wigner delay.

1 Introduction

The attosecond (1 as=10^{-18} s) time domain is of particular interest to study photo-induced processes in matter because it is well suited for initiating and observing the electron motion on their natural timescale [1–3]. From the simplest helium atom with only two electrons to multi-electronic systems such as neon, argon, and xenon, photoionization dynamics has been studied at ultrafast timescale providing a glimpse of electron correlation in flat continuum [4, 5], near Fano resonance [6, 7] and even for spin-spin interactions [8]. Compared to atoms, molecules have nuclear degrees of freedom making them an ideal choice to probe multi-center potentials with different molecular geometries. The broad diversity of available molecular systems provides a plethora of opportunities for understanding coherent electron dynamics [3]. Consequently, attosecond time-resolved experiments in molecules have seen an unprecedented development over the past few years [9–21].

Usually, the experiment employs an attosecond pulse (or pulse train) with a near infrared (NIR) light pulse stabilized with interferometric precision. One of the main protocols is the Reconstruction of Attosecond Beating by Resonant Two-photon transitions (RABBIT). It offers both spectral and temporal resolution across the attosecond timescale [5, 22]. It consists in measuring the photoelectron spectrum as a function of the delay between the attosecond pulse train (APT) and the NIR pulse with interferometric stability. The APT is produced via the high harmonic generation (HHG) process. It results in high odd-order harmonics of the NIR central frequency (ω_0) as shown in Fig. 1(b) and (c). Ionization can take place for the harmonics that have higher

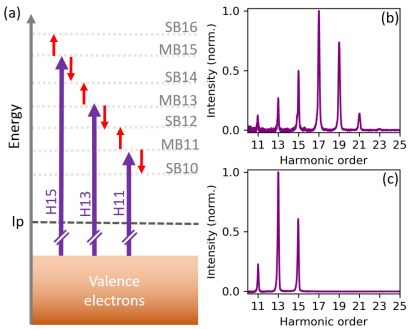

Fig. 1 (a) RABBIT protocol used in the present ionization time delay measurements (see text for details). Typical XUV spectrum obtained from high-order harmonic generation in Xenon using (b) Al and (c) Sn filter.

energy than the ionization potential of the electronic state of a target. The corresponding photoelectron channels are named main bands (MB). When the APT is dressed by an overlapping NIR pulse, new photoelectron channels appear between the MB leading to the creation of sidebands (SB) as shown in Fig. 1(a). When the delay τ between the APT and the NIR pulse is varied, the

SB and MB intensities of order m ($I_m(\tau)$) oscillate at twice the NIR frequency,

$$I_m(\tau) = \mathcal{A}_m + \mathcal{B}_m \cos(2\omega_0\tau - \phi_m), \tag{1}$$

with $\mathcal{A}_m$ and $\mathcal{B}_m$ being dependent on the experimental conditions. For the sidebands, their oscillation phases ϕ_m can usually be decomposed in three different phase terms [23, 24] as follows

$$\phi_m = \Delta\varphi_m^{APT} + \Delta\varphi_m^{cc} + \Delta\varphi_m^{i}. \tag{2}$$

The first term is named the *attochirp*. It corresponds to the difference between phases of the surrounding harmonics ($\Delta\varphi_m^{APT} = \varphi_{m+1}^{APT} - \varphi_{m-1}^{APT}$). The measurement of the harmonic phases φ^{APT} (extracted from ϕ_m Eq. 2) combined with the measurement of their respective amplitudes (see Fig. 1(b) and (c)) allow to reconstruct the temporal profile via Fourier transformation as shown in Fig. 2.

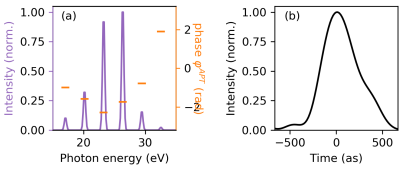

Fig. 2 Reconstructed attosecond pulse train in (a) the spectral and (b) the temporal domain taken from [25].

The second term φ_m^{cc} is the continuum-continuum phase. It corresponds to the phase induced by the NIR pulse that can be calculated theoretically [23]. The third term (φ_m^{i}) corresponds to the ionization phase. This last term carries the information on the electron dynamics. According to the Wigner theory [26, 27], the derivative of this phase with respect to the energy ($\tau_w = \hbar\Delta\phi_m^i/\Delta E = [\phi_{m+1}^i - \phi_{m-1}^i]/2\omega_0$) can be semi-classically understood as the delay in photoionization. It is due to the excursion of the ionized photoelectron wavepacket through the potential of the residual ion. By calibrating the two first phase terms on a reference target, the ionization time delay τ_w can be extracted using the RABBIT protocol [24].

In few-atom molecules, some of the electronic states have similar ionization potentials and can be ionized by a single XUV photon energy [28]. In this case, the RABBIT measures the oscillations originating from different electronic states at the same time, *i.e.* under the exact same experimental conditions (same $\Delta\varphi_m^{APT}$). By comparing the oscillations, the ionization time delay difference between the electronic states can be extracted. This method seems to be experimentally limited for growing molecular sizes where the number of electronic states and vibrational levels congest the photoelectron spectrum. For many-atom systems, even a single XUV-photon produces a series of broadband structures in the photoelectron spectrum [29]. In that case, the spectroscopic

details of an individual electronic state can be lost within the overall photoelectron features. However, the channel with the highest electron kinetic energy remains isolated in energy from the others, and the valence orbitals delocalized among an extended molecular potential can lead to a collective electron behavior.

In this paper, we address the question of electron dynamics in growing molecular size using experiments from our team and mainly performed in our laboratory. We show several attosecond electronic dynamics for few-atom molecules, with some perspectives in many-atom molecules. Also, we introduce a general analytical scattering model to predict the ionization time delay around a resonance in the photoionization continuum.

2 Ionization of few-atom systems

Attosecond time-resolved measurements of few-atom molecules are known to provide useful insights onto the molecular photoionization processes, especially for correlated electron-nuclear motion [9–20]. These experiments showed that the variation of the ionization time delay as a function of the photon energy can be sensitive to the structures of the ionization continuum, such as resonances and autoionization states.

In this regard, one of the well-known mechanisms that leads to a significant change in the photoionization continuum is the shape resonance [30]. A prototypical example is the nitrogen (N_2) σ shape resonance [30–32]. Ionization of the highest-occupied-molecular-orbital (HOMO) in N_2 corresponds to the removal of a $3\sigma_g$ electron of the neutral molecule. The resulting cross-section for the X state manifests itself as a peak-like structure around 30 eV photon energy, due to the underlying shape resonance. The A state (HOMO-1) corresponds to the removal of a $1\pi_u$ electron, which has a flat continuum around 30 eV. Hence, it can act as an internal reference to study the effect of the shape resonance in the X state in the temporal domain. Recently, the relative ionization time delay between the X and A states has been measured around the shape resonance in N_2 using two different experimental approaches with two different setups. The results are shown in Fig. 3. The first experimental approach [11] used the RABBIT technique under its original form [22], with a high spectral resolution (magnetic bottle electron spectrometer). The results shed light on the sensitivity of the shape resonance on the different molecular bond lengths resolving the vibrational levels of the X and A states. The second experimental approach is a variant of the RABBIT method [10, 33] introduced by Laurent *et al.* [34]. It consists of using a second harmonic (wavelength: 400 nm) as a dressing field instead of the fundamental one at 800 nm. It requires measuring the angularly resolved photoelectron spectrum, which can be performed with a velocity map imaging spectrometer [36]. Compared to the standard RABBIT protocol, this approach avoids the overlap between the X and A channels, while allowing to retrieve the same phase information about

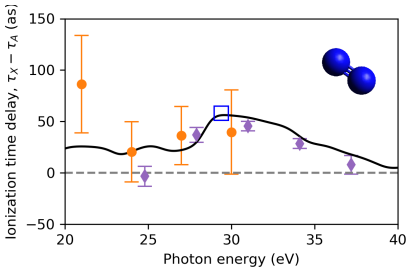

Fig. 3 Ionization time delays around the shape resonance of nitrogen molecule. Purple solid diamonds are measurements from Nandi *et al.* [11] using the RABBIT protocol. The orange solid circles represent measurements from Loriot *et al.* [10, 33] performed using a variant of the RABBIT protocol [34] that circumvents the overlapping signal from the X and A states. The solid black line is a recent two-photon transition calculation based on R-matrix theory [35]. The open square represents the τ_{sr} value obtained from the analytical model close to the maximum of the resonance.

the underlying electron dynamics. Despite being different in their implementation, the photoionization time delays obtained from these two experiments match quantitatively, demonstrating the robustness of the findings (see Fig. 3). Furthermore, the experimental results are compared with recent calculations, where the relevant two-photon matrix elements for N_2 are directly calculated for the X and A states through the R-matrix approach [35]. This numerical method does not involve the phase decomposition approximation (see Eq. 2), which usually accompanies the RABBIT analysis. The experimental data are found in excellent agreement with the theory. As shown in Fig. 3, independently of the approach, the theoretical and the experimental ionization time delay show a clear maximum around 30 eV photon energy.

The relative ionization time delay between the two states that reaches up to 50 attoseconds that can be attributed to the presence of the $3\sigma_g^{-1}$ shape resonance in the X state [31, 32] of N_2^+. Semi-classically, a shape resonance corresponds to the resonant trapping of an electron in the continuum by a centrifugal potential barrier. The barrier originates from a high angular quantum number in the Hamiltonian: $\ell(\ell+1)/r^2$, where r is the average distance between the photoelectron and the ionic core [30]. In contrast with the flat continuum case, this trapped electron can tunnel out to the continuum with a significant delay. The shape resonance usually manifests itself as a broad peak (typically a few eV wide) in the photo-absorption cross-section. In general, the parameters dictating the shape resonance are highly sensitive to the structure of the centrifugal potential responsible for trapping the photoelectron before it can reach the continuum [11]. For example, the resonance width with a full-width-at-half-maxima (FWHM) Γ, provides an estimate of the associated trapping lifetime. Following the Breit-Wigner formalism, for a quasi-bound state close to the resonance energy E_0, the scattering phase (η_ℓ) corresponding to the ℓ^{th}

partial wave can be written as

$$\eta_\ell = \eta_\ell^0 + \tan^{-1}\left[\frac{\Gamma}{2(E_0 - E)}\right], \tag{3}$$

with E being the electron kinetic energy and η_l^0 the scattering phase in the absence of resonances. Following the formalism of Wigner [26], the corresponding ionization time delay close to the resonance ($E \approx E_0$) becomes,

$$\tau_\ell = 2\hbar\frac{d\eta_\ell}{dE} = 2\hbar\frac{d\eta_l^0}{dE} + \frac{4\hbar}{\Gamma}. \tag{4}$$

Here, $2\hbar\frac{d\eta_l^0}{dE}$ represents the time delay in the absence of resonances. This term is usually of similar magnitude for the X and A states and thus, when taking the difference in time delay between the two states, its contribution is weakened (see Fig. 3 off-resonance). The term $4\hbar/\Gamma$ corresponds to the contribution of the shape resonance. For molecular photoionization, the target is usually randomly oriented. In order to take it into account, the values in Eq. 4 need to be averaged over all possible orientations. Following the procedure described by Nussenzveig [37], we can write the time delay averaged over all partial waves as,

$$\tau = \frac{1}{\pi a^2}\sum_\ell \tau_\ell \frac{(2\ell+1)\lambda^2}{4\pi}. \tag{5}$$

Here, πa^2 represents the total cross-section associated with a scattering center having radius a. Near the resonance, the de-Broglie wavelength, λ of the emitted photoelectron can be considered close to the size of the photoionized molecule that, in turn, can be approximated to a. Thus, the Wigner-delay associated with a specific partial wave ℓ_r responsible for the resonance can be written as

$$\tau_r \approx \frac{(2\ell_r + 1)}{\pi^2}\frac{\hbar}{\Gamma}. \tag{6}$$

For the X state in N_2^+, the cross-section close to the resonance maxima is dominated by the f-wave ($\ell_r = 3$) with $\Gamma \approx 8$ eV [32]. Combining all these, τ_r is found to be 58 as that matches well both the experimental values and the R-matrix calculations close to the resonance maxima (see Fig. 3). This result is consistent with the assumption that the experimental two-photon time delay difference between the X and the A states provides an effective measure of the Wigner time delay associated with the shape resonance of the X state. Despite its simplistic nature, the analytical model provides the physical description of the underlying processes at play. In addition, close to the resonance the Wigner time delay is proportional to the lifetime $\hbar/\Gamma$ of the resonance state, which can also be anticipated from the energy-time uncertainty principle. The ionization time delays of N_2 provide unique opportunities to study the properties of the ionization continuum.

Depending on the molecule under consideration, different features can be observed in the ionization continuum. Much like diatomic molecules, few-atom molecules can also have only a few and well defined contributions in their photoelectron spectra following XUV ionization [28]. A solution to increase the molecular complexity from nitrogen molecule is to consider the C_2H_{2x} (x =1, 2, 3) family of molecules. For instance, acetylene (C_2H_2) has the same number of electrons and the same $\mathcal{D}_{\infty h}$ symmetry as the nitrogen molecule. Despite their similarities, they have different attosecond responses, as it will be shown in a forthcoming paper. Here, we present some new promising results on the $x = 2$ case: the ethylene molecule (C_2H_4) using the RABBIT protocol. Following the addition of the hydrogen atoms, the molecule has a planar geometry with its symmetry group being $\mathcal{D}_{2h}$ in its ground state. The ionization time delays of electrons coming from different molecular orbitals in C_2H_4 are investigated using the RABBIT protocol with angular resolution.

The photoionization of ethylene by near-monochromatic XUV light from synchrotron sources leads to a complex photoelectron spectrum with several electronic bands that are a few eV wide and- contain vibrational structures [38, 39]. The two outermost states, X and A, correspond to the ionization of the $1b_{3u}$ and $1b_{3g}$ orbitals in C_2H_4 with C=C and C–H character and have ionization potentials of 10.5 and 12.8 eV respectively. These electronic states have different anisotropies in the photoelectron angular distributions with respect to the polarization axis. At photon energies around 22 eV, the electrons from the X state are principally ionized along the laser polarization, with an anisotropy parameter $\beta_2(X) \approx 1$, whereas, the electrons from the A state shows a near-homogeneous angular distribution $\beta_2(A) \approx 0$ [40, 41].

The implementation of the RABBIT scheme (see Fig. 1(a)) in C_2H_4 with the valence photoelectron spectra leads to a strong spectral overlapping between different contributions. To extract the SB oscillations separately, one needs to apply deconvolution algorithms [42]. To reduce this congestion problem, a solution is to limit the number of channels by using a small number of harmonics. In our case, we used a metallic tin (Sn) filter that isolates the harmonics 11^{th}, 13^{th}, and 15^{th} (see Fig. 1(c)). Because of the XUV spectral distribution, the dominant sideband oscillation is the SB14, with relatively weak oscillations observed in the case of SB12. Within the RABBIT protocol, the NIR dressing field does not ionize the target but redistributes the photoelectrons by one photon transition. As the number density of electrons created by the XUV photons remains constant, an increase in the SB yield implies a decrease of the surrounding MB intensities as shown in [43], in the case of a single harmonic RABBIT-like experiment. The MB intensity oscillates with the same frequency $2\omega_0$, but in phase opposition compared to the SB intensity. In the absence of an interfering pathway, a sideband is a weak replica of the mainband. When the magnitude of the mainband is oscillating, its replica also oscillates in phase. As shown in Fig. 1(a), both SB12 and SB14 arise due to the interference between two pathways, while SB10 and SB16 are just weak replicas of MB11 and MB15, respectively. As the intensity of MB15 oscillates

in phase opposition compared to SB14, the SB16 intensity that is a duplication of MB15 also oscillates in phase opposition compared to SB14. In other words, the phase of the SB14 can be read on MB15 and SB16 considering an additional π-shift.

According to Fig. 1(a), the highest measurable kinetic energy oscillation comes from the SB16 of the X state (SB16(X)). This oscillation can easily be isolated experimentally under background-free conditions. As explained above, this oscillation corresponds to a π-shifted replica of the SB14(X). The next measurable oscillation is the unresolved mixture between the SB16(A) and the oscillation of the MB15(X). In a first approximation, the oscillation phase of the mixture corresponds to the mean phase weighted by the oscillation amplitude of their respective channels. Hence any difference in this phase indicates the relative tendency in the ionization time of the A state compared to the X state. As shown in Fig. 4(a), the relative intensity of the RABBIT oscillations

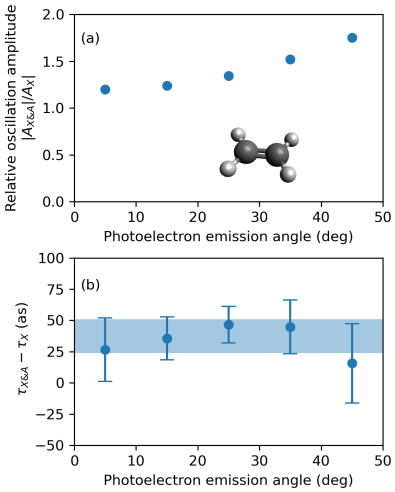

Fig. 4 Relative angle-resolved ionization time delay between the two outer valence states of ethylene. Angle-resolved oscillations (a) amplitude ratio and (b) phase difference (converted in time delay) at $2\omega_0$ between energy regions where the X state is measured alone and mixed with the A state at 22 eV photon energy.

varies with the emission angle with respect to the polarization axis. This is attributed to the fact that the photoemission anisotropy of the X state is more localized along the laser polarization. The angularly resolved ionization time delays for these two regions are shown in Fig. 4(b). Overall, a difference of (38±15) as is measured between the two regions, which does not significantly depend on the photo-emission angle. The uncertainties are evaluated from the stability of the phase measurement within the energy range of interest. Due to the close proximity of the kinetic energy windows chosen here, the difference in τ_{cc} values between the two regions is limited to ∼8 as [23]. The observed

time delay difference is purely of molecular nature that originates from a difference in ionization time delays between the two ionic states, X and A. Since the anisotropy parameter (β_2) differs significantly for the two orbitals in the photon energy range reported here [44], we speculate that the difference is a result of different partial waves associated with the ionization process for the two states. For photoionization time delays, Eq. 5 implies that even if λ and a are close for the two states, the quantity τ_ℓ can depend significantly on the partial wave that contributes the most. Note that this expression, along with the general definition of ℓ-dependent Wigner delay, holds for any molecular target. Additional calculations are necessary to elucidate the exact photoionization mechanism, for instance, what is the influence of the autoionization states that are close in energy [44], and how it affects the corresponding time delays. Further angularly resolved deconvolution algorithms could separate the contributions and provide a relative ionization time delay measurement. We hope that these results will motivate the community in pushing the boundary of attosecond science both experimentally and theoretically.

3 Ionization of many-atom systems

As the number of atoms increases in a molecule, the valence band becomes more complex. The ionization of a many-atom system at a given XUV photon energy results in a complex assembly of continuous bands in the photoelectron spectrum from different electronic states. A number of electron emission mechanisms such as resonances, autoionization states, satellite states, and thermoionic processes can be found in the measured spectrum [29, 45]. The diversity of physical mechanisms opens up new questions associated with electron scattering in such broad multi-center potentials. It provides ample opportunities in attosecond science to study electron dynamics in large molecular systems, such as collective electron motions.

Electron dynamics in many-atom molecules face number of theoretical and experimental challenges. Only few experiments in the temporal domain are reported in many-atom molecules [46, 47] or molecular clusters [21]. Alternatively, promising solutions in the spectral domain [14, 48] bring complementary tools to track the electron dynamics. In the following, we present examples of measurements performed in many-atom systems in the temporal ($C_{10}H_x$) and in the spectral domain (C_{60}). In both cases, we show that it is possible to extract an experimental signal that reflects the electron dynamics at the attosecond timescale in large molecules.

Due to its high degree of symmetry, C_{60} is an archetypal example of many-atom systems. It contains 240 electrons in its valence band, implying at least 120 contributions in the photoelectron spectrum distributed over a few tens of eV. In the XUV domain, this molecule presents a surface plasmon resonance (SPR) well above its ionization potential. The SPR at around 20 eV photon energy corresponds to a collective oscillation of the delocalized π electrons [49].

In the time domain, experiments on the electron dynamics in C_{60} are emerging [46]. In the spectral domain, Barillot *et al.* [48] have shown that the electron correlation that governs the SPR has a strong influence on both the photoelectron anisotropy distribution and the photoionization time delay. On one hand, a sudden drop in the anisotropy parameter β_2 appears around the SPR at 20 eV photon energy (see Fig. 5 (a) and (b)). Such measurements are compared with TDLDA (time-dependent local density approximation) calculations. Experiment and theory are found in good agreement only when the electronic correlation term responsible for the SPR is considered. On the other

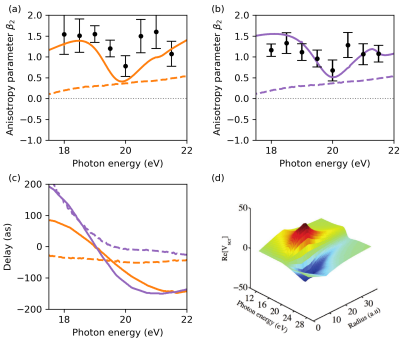

Fig. 5 Effect of the plasmon resonance in C_{60} (adapted from [48]). Variation of the experimental anisotropy parameter β_2 of (a) HOMO and (b) HOMO-1 as a function of the photon energy. Dots with error bars represent the experimental values, the lines correspond to the TDLDA calculations including (solid orange line) or not (dashed purple line) the plasmon resonance. (c) Ionization time delay for the HOMO (orange) and the HOMO-1 (purple) from the calculation with considering (solid line) or not (dash line) the SPR. (d) Real part of the SPR screening potential modeled as a function of the photon energy and the C_{60} cage radius.

hand, the ionization time delay can be extracted from the TDLDA calculations following the above-mentioned Wigner approach [26]. For the anisotropy distribution, the consideration of the SPR also implies strong differences in the ionization time delay at the attosecond timescale (see Fig. 5 (c)). To go deeper onto the common origin of such two observables (β_2 and ionization delays), a simple 1D model has been developed under WKB (Wentzel-Kramers-Brillouin) approximation. In this model, the SPR appears as an additional radial screening potential (Fig. 5 (d)) in the Hamiltonian [48]. For the TDLDA calculations, the consideration of this term is mandatory to reproduce the anisotropy and to predict similar variations of the ionization time around the SPR. This shows that some spectroscopic features can carry signatures of the collective electronic dynamics at ultrashort timescale.

In many-atom molecules, after XUV photoionization, an outgoing electron scatters in a large molecular potential before reaching the continuum. At a first glance, one might expect that the ionization time delay simply increases with the size of the molecular potential [21]. This intuitive statement implicitly considers a spherically symmetric potential. This opens up the general question

on the dependency of the photoionization time delay on the molecular symmetry. To address this point, we have investigated the differences in ionization time delay between two $C_{10}H_x$ molecules [47]. Adamantane ($C_{10}H_{16}$) has a diamondoid cage-like structure, that can be described as a pseudo-spherical scattering potential. In contrast, naphthalene ($C_{10}H_8$) has a robust 2D planar structure in its ground state. Considering the delocalized character of the electronic states in the valence band, it can be expected that the symmetry of the molecular potential influences the scattering of the escaping electrons which, in turn, affects the ionization time delays of the valence band.

The ionization time delay can be investigated through the RABBIT protocol (Fig. 1(a)). Since the naphthalene and adamantane valence band is far more complex than the C_2H_4 case, it makes the experiment quite more challenging. As shown in Fig. 6, performing RABBIT measurement using naphthalene as a target produces a highly congested photoelectron signal, with only a few percent $2\omega_0$ oscillations [50]. Since all the electrons in the valence band follow

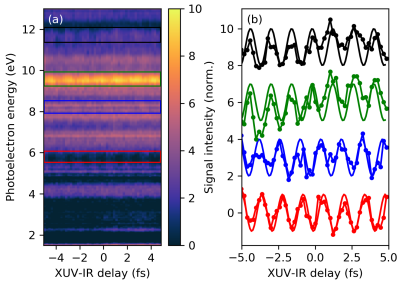

Fig. 6 RABBIT measurement in Naphthalene adapted from [50] with (a) the photoelectron spectrum as a function of the time delay between the XUV and the NIR pulse and (b) variation of the signal for the kinetic energy ranges indicated by the rectangles with the corresponding color in (a).

the RABBIT scheme, the resulting oscillation is the sum of all the individual channels. The resulting oscillation is weak, and the perfect cancellation can only appear accidentally. Independently of the spectral congestion, the oscillation at the highest kinetic energy is always measured under background-free conditions. As shown in Fig. 1(a), it originates from the outer electronic state with the ionization channel leading to the highest kinetic energy. The RABBIT oscillation at this kinetic energy is free from any spectral congestion. Using this channel, it has been found that the ionization time delays of the naphthalene molecules for the three outermost electronic states are few tens of attosecond lower than the ones of adamantane for the photon energy range of 20-30 eV [47].

Such experimental results can be explained by the distribution of the atoms within the molecule, which significantly alters the scattering in the short range potential. Being a 2D molecule, the residual hole produced in naphthalene at the instant of ionization is spread over the molecular plane. Compared to a

point-like charge (e.g., atomic ion), the extended charge distribution in a 2D molecule is less attractive towards the photoelectron, leading to a negative ionization time delay. This negative delay can be understood as a repulsive term in the molecular potential due to a quadrupole contribution coming from the planar nature of the hole distribution in the naphthalene cation. Such conclusions are supported by SE-DFT (Static Exchange Density Functional Theory) calculations and a scattering model that considers the effect of the quadrupole term in the photoionization time delay. Our findings establish that attosecond metrology of complex molecules could be a powerful tool for exploring the rich information about the nature of effective short range potential in many-atom systems.

4 Conclusion

Tracking the electron dynamics at the attosecond timescale is a promising physical observable exalted by the naturally broad diversity of molecular systems. The measurement of the amplitude and phase of the photoelectron wavepacket in 'real-time' is a sensitive probe of the molecular potential down to the ångstr̈om length-scale. They can be used as a precise probe of the state of the quantum system at a well-defined instant. In our attoscience laboratory in Lyon, we carried out angle-resolved measurements of ionization time delays on few-atom systems [10] as well as large many-atom molecules such as fullerenes [49] and hydrocarbons [47, 50].

The few-atom molecules have a limited number of electronic states with different symmetries that can be ionized with an XUV photon. In that case, the electronic states can be compared with each other following a similar protocol as in the atomic case [24]. This allows us to study in details the structure of the continuum using an internal reference. In contrast, in many-atom systems, many electronic states are involved forming several overlapping bands in the photoelectron spectrum. As shown with C_{60}, some electronic dynamics have signatures in the anisotropy distribution of the electrons. In the temporal domain, the spectral congestion is reinforced by the dressing field used in the RABBIT method. However, in many-atom molecules collective effects can drive the overall dynamics. In that case, the ionization time delay measurement can be associated with molecular properties such as the screening potential that appears due to the electron correlation at the vicinity of a plasmon resonance, or to the global symmetry of the molecule. Attosecond technology provides new tools to explore microscopic details of the many-atom molecules. The frontier between few- to many-atom molecules depends on the photon energy range and the quantum system under consideration. The quest of increasing the molecular size can eventually contribute to a bridge between isolated systems in gas-phase, clusters [21], nano-particles [51] and solid-state physics [52, 53].

Acknowledgments

We thank F. Lépine and E. Constant for fruitful discussions. We acknowledge the support of CNRS, ANR-16-CE30-0012 "Circé", ANR-15-CE30-0001 "CIMBAAD", the Fédération de recherche André Marie Ampère and the European COST Action AttoChem (CA18222) and the GDR-UP.

References

[1] P. Agostini and L. F. DiMauro, "The physics of attosecond light pulses," *Reports on Progress in Physics*, vol. 67, pp. 813–855, may 2004.

[2] F. Krausz and M. Ivanov, "Attosecond physics," *Rev. Mod. Phys.*, vol. 81, pp. 163–234, Feb 2009.

[3] F. Lépine, M. Y. Ivanov, and M. J. J. Vrakking, "Attosecond molecular dynamics: fact or fiction?," *Nature Photonics*, vol. 8, p. 195, 2014.

[4] M. Schultze *et al.*, "Delay in photoemission," *Science*, vol. 328, no. 5986, pp. 1658–1662, 2010.

[5] M. Isinger, R. J. Squibb, D. Busto, S. Zhong, A. Harth, D. Kroon, S. Nandi, C. L. Arnold, M. Miranda, J. M. Dahlström, E. Lindroth, R. Feifel, M. Gisselbrecht, and A. L'Huillier, "Photoionization in the time and frequency domain," *Science*, vol. 358, no. 6365, pp. 893–896, 2017.

[6] M. Kotur *et al.*, "Spectral phase measurement of a fano resonance using tunable attosecond pulses," *Nat Commun.*, vol. 7, p. 10566, 2016.

[7] V. Gruson, L. Barreau, A. Jiménez-Galan, F. Risoud, J. Caillat, A. Maquet, B. Carré, F. Lepetit, J.-F. Hergott, T. Ruchon, L. Argenti, R. Taïeb, F. Martín, and P. Salières, "Attosecond dynamics through a fano resonance: Monitoring the birth of a photoelectron," *Science*, vol. 354, no. 6313, pp. 734–738, 2016.

[8] S. Zhong *et al.*, "Attosecond electron–spin dynamics in Xe 4d photoionization," *Nat Commun.*, vol. 11, p. 5042, 2020.

[9] L. Cattaneo, J. Vos, R. Y. Bello, A. Palacios, S. Heuser, L. Pedrelli, M. Lucchini, C. Cirelli, F. Martín, and U. Keller, "Attosecond coupled electron and nuclear dynamics in dissociative ionization of H_2," *Nature Physics*, vol. 14, pp. 733– 738, 2018.

[10] V. Loriot, A. Marciniak, S. Nandi, G. Karras, M. Hervé, E. Constant, E. Plésiat, A. Palacios, F. F Martín, and F. Lépine, "High harmonic generation-2ω attosecond stereo-photoionization interferometry in N_2," *J. Phys. Photonics*, vol. 2, p. 024003, 2020.

[11] S. Nandi, E. Plésiat, S. Zhong, A. Palacios, D. Busto, M. Isinger, L. Neoričić, C. L. Arnold, R. J. Squibb, R. Feifel, P. Decleva, A. L'Huillier, F. Martín, and M. Gisselbrecht, "Attosecond timing of electron emission from a molecular shape resonance," *Sci. Adv.*, vol. 6, no. 31, p. eaba7762, 2020.

[12] J. Vos, L. Cattaneo, S. Patchkovskii, T. Zimmermann, C. Cirelli, M. Lucchini, A. Kheifets, A. S. Landsman, and U. Keller, "Orientation-dependent stereo wigner time delay and electron localization in a small molecule," *Science*, vol. 360, no. 6395, pp. 1326–1330, 2018.

[13] X. Gong, W. Jiang, J. Tong, J. Qiang, P. Lu, H. Ni, R. Lucchese, K. Ueda, and J. Wu, "Asymmetric attosecond photoionization in molecular shape resonance," *Phys. Rev. X*, vol. 12, p. 011002, Jan 2022.

[14] F. Holzmeier, J. Joseph, J. C. Houver, M. Lebech, D. Dowek, and R. R. Lucchese, "Influence of shape resonances on the angular dependence of molecular photoionization delays," *Nature Communications*, vol. 12, p. 7343, 2021.

[15] M. Huppert, I. Jordan, D. Baykusheva, A. von Conta, and H. J. Wörner, "Attosecond delays in molecular photoionization," *Phys. Rev. Lett.*, vol. 117, p. 093001, 2016.

[16] I. Jordan, M. Huppert, D. Rattenbacher, M. Peper, D. Jelovina, C. Perry, A. von Conta, A. Schild, and H. J. Wörner, "Attosecond spectroscopy of liquid water," *Science*, vol. 369, no. 6506, pp. 974–979, 2020.

[17] A. Kamalov, A. L. Wang, P. H. Bucksbaum, D. J. Haxton, and J. P. Cryan, "Electron correlation effects in attosecond photoionization of CO_2," *Phys. Rev. A*, vol. 102, p. 023118, Aug 2020.

[18] H. Ahmadi, E. Plésiat, M. Moioli, F. Frassetto, L. Poletto, P. Decleva, C. D. Schröter, T. Pfeifer, R. Moshammer, A. Palacios, F. Martín, and G. Sansone, "Attosecond photoionisation time delays reveal the anisotropy of the molecular potential in the recoil frame," *Nature Communications*, vol. 13, p. 1242, 2022.

[19] S. Biswas, B. Förg, L. Ortmann, J. Schötz, W. Schweinberger, T. Zimmermann, D. Pi, L. Baykusheva, H. Masood, I. Liontos, A. M. Kamal, N. G. Kling, A. F. Alharbi, M. Alharbi, A. M. Azzeer, G. Hartmann, H. J. Wörner, Landsman, and M. F. A. S. Kling, "Probing molecular environment through photoemission delays," *Nature Physics*, vol. 16, pp. 778–783, 2020.

[20] S. Heck, D. Baykusheva, M. Han, J.-B. Ji, C. Perry, X. Gong, and H. J. Wörner, "Attosecond interferometry of shape resonances in the recoil

frame of CF_4," *Sci. Adv.*, vol. 7, no. 49, p. eabj8121, 2021.

[21] X. Gong, S. Heck, D. Jelovina, C. Perry, K. Zinchenko, R. Lucchese, and H. J. Wörner, "Attosecond spectroscopy of size-resolved water clusters," 2022.

[22] P. M. Paul, E. S. Toma, P. Breger, G. Mullot, F. Augé, P. Balcou, H. G. Muller, and P. Agostini, "Observation of a train of attosecond pulses from high harmonic generation," *Science*, vol. 292, no. 5522, pp. 1689–1692, 2001.

[23] J. M. Dahlström, D. Guénot, K. Klünder, M. Gisselbrecht, J. Mauritsson, A. L'Huillier, A. Maquet, and R. Taïeb, "Theory of attosecond delays in laser-assisted photoionization," *Chem. Phys.*, vol. 414, pp. 53–64, 2013.

[24] K. Klünder *et al.*, "Probing single-photon ionization on the attosecond time scale," *Phys. Rev. Lett.*, vol. 106, p. 143002, Apr 2011.

[25] V. Loriot *et al.*, "Angularly resolved rabbitt using a second harmonic pulse," *J. Opt.*, vol. 19, p. 114003, 2017.

[26] E. P. Wigner, "Lower limit for the energy derivative of the scattering phase shift," *Phys. Rev.*, vol. 98, pp. 145–147, 1955.

[27] R. Pazourek, S. Nagele, and J. Burgdörfer, "Attosecond chronoscopy of photoemission," *Rev. Mod. Phys.*, vol. 87, pp. 765–802, Aug 2015.

[28] K. Kimura, S. Katsumata, Y. Achiba, T. Yamazaki, and S. Iwata, *Handbook of HeI Photoelectron Spectra of Fundamental Organic Molecules.* Japan Scientific Societies Press, Tokyo, 1981.

[29] U. Becker and D. A. Shirley, eds., *VUV and Soft X-Ray Photoionization.* Springer New York, NY, 1996.

[30] M. Piancastelli, "The neverending story of shape resonances," *Journal of Electron Spectroscopy and Related Phenomena*, vol. 100, no. 1, pp. 167–190, 1999.

[31] R. R. Lucchese and R. W. Zurales, "Comparison of the random-phase approximation with the multichannel frozen-core hartree-fock approximation for the photoionization of N_2," *Phys. Rev. A*, vol. 44, pp. 291–303, Jul 1991.

[32] P. Hockett, E. Frumker, D. M. Villeneuve, and P. B. Corkum, "Time delay in molecular photoionization," *Journal of Physics B: Atomic, Molecular and Optical Physics*, vol. 49, p. 095602, apr 2016.

[33] V. Loriot, A. Marciniak, S. Nandi, G. Karras, M. Hervé, E. Constant, E. Plésiat, A. Palacios, F. Martín, and F. Lépine, "Attosecond interferometry using a HHG-2ω_0 scheme," *Studia UBB Physica*, vol. 65, pp. 35–47, 2020.

[34] G. Laurent, W. Cao, H. Li, Z. Wang, I. Ben-Itzhak, and C. L. Cocke, "Attosecond control of orbital parity mix interferences and the relative phase of even and odd harmonics in an attosecond pulse train," *Phys. Rev. Lett.*, vol. 109, p. 083001, Aug 2012.

[35] J. Benda, Z. Mašín, and J. D. Gorfinkiel, "Analysis of rabitt time delays using the stationary multiphoton molecular R-matrix approach," *Phys. Rev. A*, vol. 105, p. 053101, May 2022.

[36] A. T. J. B. Eppink and D. H. Parker, "Velocity map imaging of ions and electrons using electrostatic lenses: Application in photoelectron and photofragment ion imaging of molecular oxygen," *Rev. Sci. Instrum.*, vol. 68, no. 9, pp. 3477–3484, 1997.

[37] H. M. Nussenzveig, "Time delay in quantum scattering," *Phys. Rev. D*, vol. 6, pp. 1534–1542, Sep 1972.

[38] G. Bieri and L. Åsbrink, "30.4-nm He(II) photoelectron spectra of organic molecules: Part I. hydrocarbons," *Journal of Electron Spectroscopy and Related Phenomena*, vol. 20, no. 1, pp. 149–167, 1980.

[39] J. G. Brennan, G. Cooper, J. C. Green, M. P. Payne, and C. M. Redfern, "Relative partial photoionization cross-sections and photoelectron branching ratios of ethylene," *Journal of Electron Spectroscopy and Related Phenomena*, vol. 43, no. 3, pp. 297–305, 1987.

[40] D. Holland, M. MacDonald, M. Hayes, L. Karlsson, and B. Wannberg, "A photoelectron spectroscopy study of the valence shell photoionization dynamics of acetylene," *Journal of Electron Spectroscopy and Related Phenomena*, vol. 97, no. 3, pp. 253–263, 1998.

[41] D. Toffoli and P. Decleva, "A multichannel least-squares b-spline approach to molecular photoionization: Theory, implementation, and applications within the configuration–interaction singles approximation," *Journal of Chemical Theory and Computation*, vol. 12, no. 10, pp. 4996–5008, 2016. PMID: 27626466.

[42] I. Jordan and H. J. Wörner, "Extracting attosecond delays from spectrally overlapping interferograms," *J. Opt.*, vol. 20, p. 024013, 2018.

[43] M. Lucchini, G. D. Lucarelli, M. Murari, A. Trabattoni, N. Fabris, F. Frassetto, S. D. Silvestri, L. Poletto, and M. Nisoli, "Few-femtosecond

extreme-ultraviolet pulses fully reconstructed by a ptychographic technique," *Opt. Express*, vol. 26, pp. 6771–6784, Mar 2018.

[44] G. Fronzoni, M. Stener, and P. Decleva, "Valence and core photoionization dynamics of acetylene by td-dft continuum approach," *Chemical Physics*, vol. 298, no. 1, pp. 141–153, 2004.

[45] F. Lépine, "Multiscale dynamics of C_{60} from attosecond to statistical physics," *Journal of Physics B: Atomic, Molecular and Optical Physics*, vol. 48, p. 122002, may 2015.

[46] S. Biswas, A. Trabattoni, P. Rupp, M. Magrakvelidze, M. El-Amine Madjet, U. De Giovannini, M. Castrovilli, M. Galli, Q. Liu, E. P. Mansson, J. Schötz, V. Wanie, F. Légaré, P. Wnuk, M. Nisoli, A. Rubio, H. Chakraborty, M. Kling, and F. Calegari, "Attosecond correlated electron dynamics at C_{60} giant plasmon resonance," *Arxiv*, p. arXiv:2111.14464v1, 2022.

[47] V. Loriot, A. Boyer, S. Nandi, E. Plésiat, A. Marciniak, M. Lara-Astiaso, A. Palacios, P. Decleva, F. Martín, and F. Lépine, "Attosecond metrology of 2D charge distribution in molecules," *arXiv*, vol. 10.48550, p. 2209.02445, 2022.

[48] T. Barillot *et al.*, "Angular asymmetry and attosecond time delay from the giant plasmon resonance in C_{60} photoionization," *Phys. Rev. A*, vol. 91, p. 033413, Mar 2015.

[49] S. W. J. Scully, E. D. Emmons, M. F. Gharaibeh, R. A. Phaneuf, A. L. D. Kilcoyne, A. S. Schlachter, S. Schippers, A. Müller, H. S. Chakraborty, M. E. Madjet, and J. M. Rost, "Photoexcitation of a volume plasmon in C_{60} ions," *Phys. Rev. Lett.*, vol. 94, p. 065503, Feb 2005.

[50] V. Loriot *et al.*, "Resolving XUV induced femtosecond and attosecond dynamics in polyatomic molecules with a compact attosecond beamline," *J. Phys. Conf. Ser.*, vol. 635, no. 1, p. 012006, 2015.

[51] L. Seiffert, Q. Liu, S. Zherebtsov, A. Trabattoni, P. Rupp, M. C. Castrovilli, M. Galli, F. Süβmann, K. Wintersperger, J. Stierle, G. Sansone, L. Poletto, F. Frassetto, I. Halfpap, V. Mondes, C. Graf, E. Rühl, F. Krausz, M. Nisoli, T. Fennel, F. Calegari, and M. Kling, "Attosecond chronoscopy of electron scattering in dielectric nanoparticles," *Nature Physics*, vol. 13, pp. 766– 770, 2017.

[52] M. Lucchini *et al.*, "Light-matter interaction at surfaces in the spatiotemporal limit of macroscopic models," *Phys. Rev. Lett.*, vol. 115, p. 137401, 2015.

[53] M. Hervé, V. Despré, P. Castellanos Nash, V. Loriot, A. Boyer, A. Scognamiglio, G. Karras, R. Brédy, E. Constant, A. G. G. M. Tielens, A. I. Kuleff, and F. Lépine, "Ultrafast dynamics of correlation bands following XUV molecular photoionization," *Nat. Phys.*, vol. 17, pp. 327–331, 2021.